
RNAGenScape: Property-Guided, Optimized Generation of mRNA Sequences with Manifold Langevin Dynamics

Danqi Liao^{*1} Chen Liu^{*1} Xingzhi Sun¹ Dié Tang¹ Haochen Wang¹ Scott Youlten¹
Srikar Krishna Gopinath¹ Haejeong Lee¹ Ethan C. Strayer¹ Antonio J. Giraldez¹ Smita Krishnaswamy¹

Abstract

Generating property-optimized mRNA sequences is central to applications such as vaccine design and protein replacement therapy, but remains challenging due to limited data, complex sequence-function relationships, and the narrow space of biologically viable sequences. Generative methods that drift away from the data manifold can yield sequences that fail to fold, translate poorly, or are otherwise nonfunctional. We present RNAGenScape, a property-guided manifold Langevin dynamics framework for mRNA sequence generation that operates directly on a learned manifold of real data. By performing iterative local optimization constrained to this manifold, RNAGenScape preserves biological viability, accesses reliable guidance, and avoids excursions into nonfunctional regions of the ambient sequence space. The framework integrates three components: ① an autoencoder jointly trained with a property predictor to learn a property-organized latent manifold, ② a denoising autoencoder that projects updates back onto the manifold, and ③ a property-guided Langevin dynamics procedure that performs optimization along the manifold. Across three real-world mRNA datasets spanning two orders of magnitude in size, RNAGenScape increases median property gain by up to 148% and success rate by up to 30% while ensuring biological viability of generated sequences, and achieves competitive inference efficiency relative to existing generative approaches.

1. Introduction

Messenger ribonucleic acids (mRNAs) have emerged as a core modality for modern therapeutics, enabling applications ranging from mRNA vaccine design and protein replacement therapy to gene regulation and synthetic biology (Pardi et al., 2018; Chaudhary et al., 2021; Qin et al., 2022; Vavilis et al., 2023). In these settings, the nucleotide sequence of an mRNA directly determines properties such as stability, translational efficiency, and ultimately protein yield. Even small sequence edits, particularly in non-coding regions such as the 5' untranslated region (UTR), can lead to substantial changes in degradation rates and ribosome loading (Castillo-Hair et al., 2024; Ma et al., 2024; Li et al., 2025). As a result, systematic optimization of the mRNA sequence has the potential to improve therapeutic efficacy, reduce dosage requirements, and expand the design space of viable mRNA-based interventions.

Despite its importance, mRNA sequence generation and optimization remains underexplored from a machine learning perspective (Castillo-Hair & Seelig, 2021; Schlusser et al., 2024). A key challenge is that viable mRNA sequences occupy a narrow and structured subset of the astronomically large ambient sequence space (Calvanese et al., 2024; Zhang et al., 2023). Random or unconstrained edits can lead to nonfunctional transcripts, while experimentally measured datasets are typically small, imbalanced, and sparsely cover the space of interest (Taubert et al., 2023; Asim et al., 2025). Moreover, sequence-function relationships in mRNA are highly nonlinear and context-dependent, making the optimization of mRNA sequences a challenging problem (Licatalosi & Darnell, 2010; Weinreb et al., 2016).

To address the challenges, we introduce RNAGenScape, a property-guided manifold Langevin dynamics framework for mRNA sequence generation built around three key components. ① An autoencoder and a property predictor, together termed an organized autoencoder (OAE), that jointly learn a latent manifold of mRNA sequences while organizing this manifold according to the target property. This latent manifold represents the subspace of biologically viable mRNA sequences rather than the

^{*}Equal contribution ¹Yale University. Correspondence to: Antonio J. Giraldez <antonio.giraldez@yale.edu>, Smita Krishnaswamy <smita.krishnaswamy@yale.edu>.

much larger Euclidean ambient space. ② A manifold projector, implemented as a denoising autoencoder, that maps data near the learned manifold onto the manifold, preventing drift toward implausible regions. To ensure robustness under sparse and imbalanced data regimes common in mRNA studies, we augment training data using SUGAR (Lindenbaum et al., 2018), which fills holes in the manifold and stabilizes manifold projection even with as few as 2,000 sequences. ③ A property-guided manifold Langevin dynamics that iteratively refines sequences by combining gradient information with stochastic exploration, while ensuring that sequences generated at every optimization step remain close to the viable mRNA manifold.

Our choice to perform iterative optimization directly on the learned data manifold, rather than adopting diffusion-based generation from Gaussian noise, is motivated by several practical considerations. **First**, mRNA sequence optimization is inherently local, where improvements are typically made relative to an existing sequence. **Second**, property-guided Langevin dynamics relies on gradients from a predictor trained on real data, and therefore staying close to the data manifold helps obtain stable and meaningful guidance. In contrast, standard diffusion and flow-matching models frequently traverse off-manifold regions during generation, leading to unstable or misleading guidance from predictors. **Third**, constraining the optimization trajectory to the manifold encourages the generated sequences to remain within biologically viable regions of sequence space. **Finally**, avoiding repeated diffusion to and denoising from a noise distribution far away from the data manifold reduces computational overhead and enables faster inference.

We evaluate RNAGenScape on three real-world mRNA datasets under diverse experimental settings. Across these datasets, RNAGenScape improves median property gain by up to 148% over state-of-the-art methods and success rates by up to 30%, while preserving biological viability and demonstrating generalization in a held-out optimization study. In addition, RNAGenScape is highly efficient with a throughput 68% higher than the fastest biological sequence optimization method.

2. Preliminaries

2.1. Manifold assumption and manifold learning

The manifold assumption (Cayton et al., 2008; Narayanan & Mitter, 2010; Fefferman et al., 2016) is a fundamental principle in machine learning which hypothesizes that high-dimensional natural data lie near a low-dimensional manifold embedded in the ambient space (Li & He, 2025). Formally, each observation $x_i \in \mathbb{R}^n$ arises from a smooth nonlinear map $\mathbf{f} : \mathcal{M}^d \rightarrow \mathbb{R}^n$ applied to a latent variable $z_i \in \mathcal{M}^d$, where $d \ll n$.

Manifold learning methods seek to recover this latent structure by constructing representations that preserve intrinsic geometry (Van Dijk et al., 2018; Moon et al., 2019; Burkhardt et al., 2021; Liu et al., 2024; Liao et al., 2024; Liu et al., 2025a;b; Sun et al., 2025; Tong et al., 2023; Zhang et al., 2025). A point is considered *on-manifold* if it lies within the range of the nonlinear map \mathbf{f} , while *off-manifold* points deviate from this structure and may correspond to invalid or adversarial samples (Rifai et al., 2011; Li et al., 2023). Thus, projecting updated points back to the manifold is critical for robustness and geometry-aware optimization (He et al., 2023b).

SUGAR (Lindenbaum et al., 2018) is a diffusion geometry-based method that learns the intrinsic geometry of the data manifold and samples uniformly along the learned geometry. When observed data are limited, augmenting training sets with SUGAR enriches the learned manifold with geometry-preserving samples, particularly in sparse regions.

Stochastic gradient descent (SGD) on Riemannian manifolds (Bonnabel, 2013) extends classical SGD by computing updates in the tangent space and mapping them back to the manifold via exponential maps or retractions. However, such methods assume an analytic form of the manifold. In contrast, the manifold underlying biological sequence space is not known in a closed form. RNAGenScape addresses this by directly *learning* the projection operator, enabling optimization on data manifolds without requiring analytic solutions.

2.2. Langevin-dynamics and beyond

Langevin Dynamics (Song & Ermon, 2019) has been employed in generative models to sample from high-dimensional data distributions using only an estimate of the score function $\nabla_x \log p(x)$. In particular, it first trains a neural network \mathbf{s}_θ to approximate the score function of data injected with Gaussian noise. Sampling is then performed via annealed Langevin dynamics, given by $\tilde{x}_t = \tilde{x}_{t-1} + \frac{\eta_t}{2} \mathbf{s}_\theta(\tilde{x}_{t-1}, \sigma_i) + \sqrt{\eta_t} \mathbf{z}_t$. Here, $\mathbf{s}_\theta(\tilde{x}_{t-1}, \sigma_i)$ is the learned score function at noise level σ_i , and η_i is the step size at that level. By gradually annealing from high to low noise, this procedure enables generation of high-quality samples without an explicit likelihood or energy model.

Neural Stochastic Differential Equations (neural SDEs) (Kidger et al., 2021), are differential equations simultaneously modeling two terms: a drift term $f(\cdot)$ depicting the true time-varying dynamics of the variable, and a diffusion term $g(\cdot)$ representing stochasticity using the Brownian motion W_t . The update rule is given by $dX_t = f(t, X_t)dt + g(t, X_t) \circ dW_t$. From a high level, Langevin dynamics is a special case of neural SDEs after discretization.

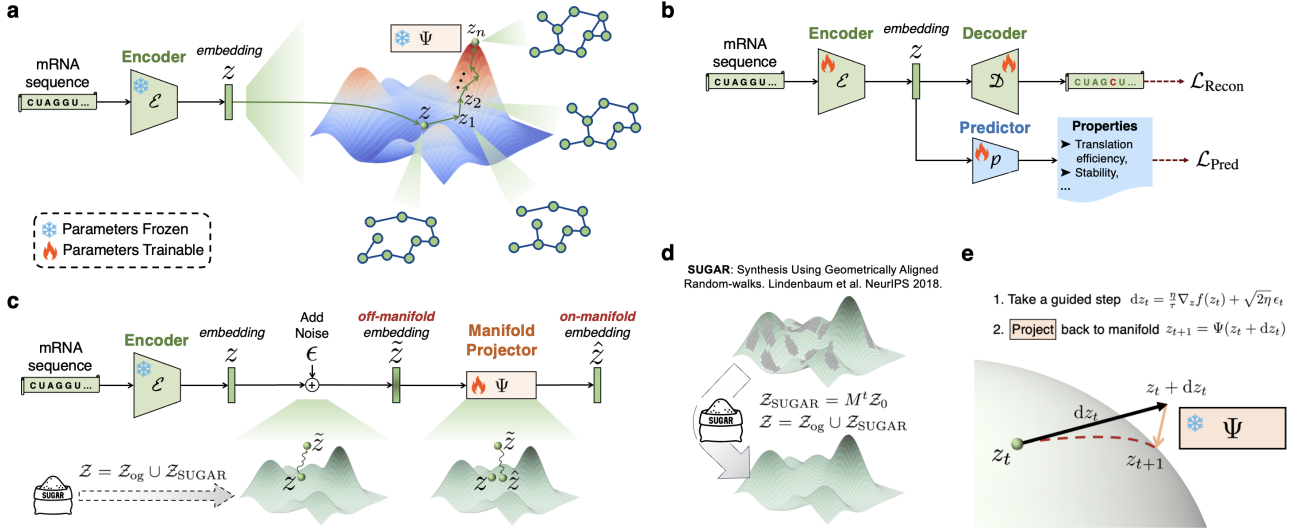


Figure 1. Schematic of RNAGenScope. **a**, We encode a given input mRNA sequence into a latent manifold organized by property, and iteratively optimize the sequence along the property landscape. The manifold projector Ψ ensures the optimization stays on or near the manifold. Notably, we can decode the intermediate optimization result after every step. **b**, The organized latent manifold is created by jointly optimizing reconstruction and property prediction objectives. **c**, The manifold projector is trained to project perturbed data points back to the manifold. **d**, For undersampled mRNA manifolds, we use SUGAR (Lindenbaum et al., 2018) to learn key dimensions in the manifold and fill undersampled regions. **e**, During optimization, the manifold projector brings off-manifold points back to the manifold.

3. RNAGenScope

The key components of our framework are **1** **OAE**: an autoencoder jointly trained with a prediction model to learn a latent manifold of mRNA sequences organized by the target property (Section 3.1 and Figure 1b), **2** **Manifold Projector**: a denoising autoencoder that brings the updated latent embeddings back to the learned data manifold during each step of optimization (Section 3.2 and Figure 1c, 1e), and **3** **Property-guided manifold Langevin dynamics**, a procedure that integrates the two aforementioned modules to enable property-guided generation (Section 3.3 and Figure 1a).

Once trained, these components allow RNAGenScope to optimize the target property, such as translation efficiency or stability, of a given mRNA sequence.

3.1. Learning a latent manifold organized by property

We begin by training an **organized autoencoder (OAE)**, where the latent manifold is implicitly structured via supervision from a property prediction task (Figure 1b).

Similar to a vanilla autoencoder (Hinton & Salakhutdinov, 2006), the encoder \mathcal{E} maps the input mRNA sequence x to a latent representation z , which is decoded by \mathcal{D} back to the sequence space. In addition to this standard architecture, a predictor \mathcal{P} infers properties \hat{y} from the embedding z . Formally, $z_i = \mathcal{E}(x_i)$, $\hat{x}_i = \mathcal{D}(z_i)$, $\hat{y}_i = \mathcal{P}(z_i)$.

The latent manifold \mathcal{Z} is thus shaped by jointly optimizing the reconstruction loss and the prediction loss (equation 1),

encouraging it to learn sequence-relevant information while being organized by the target properties. λ_{Pred} and λ_{Recon} are hyperparameters that balance between organizing the property landscape and capturing sequence information. They are empirically set as described in Supplementary Section A. Here, $x_i \in \mathbb{R}^V$ is the ground truth one-hot encoding of the nucleotide at position i in sequence x with an mRNA vocabulary of size V .

$$\begin{aligned} \mathcal{L}_{\text{OAE}} &= \lambda_{\text{Pred}} \mathcal{L}_{\text{Pred}} + \lambda_{\text{Recon}} \mathcal{L}_{\text{Recon}} \\ &= \underbrace{\lambda_{\text{Pred}} \mathbb{E}_{(x,y) \sim p_{\text{data}}} \|\hat{y}_i - y_i\|_2^2}_{\text{optimize } \mathcal{P} \text{ with MSE}} + \underbrace{\lambda_{\text{Recon}} \mathbb{E}_{x \sim p_{\text{data}}} \log \frac{\exp(\hat{x}_i, x_i)}{\sum_{v=1}^V \exp(\hat{x}_i, v)}}_{\text{optimize } \mathcal{E} \text{ and } \mathcal{D} \text{ with CrossEntropy}} \end{aligned} \quad (1)$$

3.2. Learning a module to project updates to manifold

Learning the data manifold mRNA datasets are typically scarce and unevenly sampled, which can hinder learning a faithful latent manifold directly from observed data. To mitigate this issue, we augment the latent embeddings using SUGAR (Lindenbaum et al., 2018), a diffusion geometry-based method introduced in Section 2. This augmentation enriches the learned manifold with geometry-preserving samples, particularly in sparse regions, improving robustness of subsequent manifold projection.

Specifically, this preprocessing step yields an expanded latent set: $\mathcal{Z} = \mathcal{Z}_{\text{og}} \cup \mathcal{Z}_{\text{SUGAR}}$, $\mathcal{Z}_{\text{SUGAR}} = M^t \mathcal{Z}_0$, where \mathcal{Z}_{og} are the original latent embeddings, \mathcal{Z}_0 are locally-sampled neighbors, and M^t is the sparsity-corrected Markov diffusion transition matrix applied for t steps.

Training the manifold projector To access reliable property guidance during generation and keep the generated

Algorithm 1 Manifold Projector Ψ

Input: Dataset $\mathcal{Z} = \{z_i\}_{i=1}^N$, denoiser Ψ , noise levels $\{\sigma_1, \dots, \sigma_K\}$, denoising steps K , learning rate η

for each z_i in minibatch $\{z_i\}_{i=1}^B \subset \mathcal{Z}$ **do**

Initialize $\tilde{z}^{(0)} \leftarrow z_i$

for $k = 1$ to K **do**

$\tilde{z}^{(k)} \sim C(\tilde{Z} | \tilde{Z}^{(k-1)}, \sigma_k)$

$\mathcal{L}^{(k)} = \|\Psi(\tilde{z}^{(k)}) - \tilde{z}^{(k-1)}\|_2^2$

end for

$\mathcal{L}_i = \sum_{k=1}^K \mathcal{L}^{(k)}$

$\Psi \leftarrow \Psi - \eta \nabla_{\Psi} \left(\frac{1}{B} \sum_{i=1}^B \mathcal{L}_i \right)$

end for

trajectories aligned with the latent data manifold, we introduce a manifold projector Ψ . As illustrated in Figure 1c and magnified in Figure 1e, Ψ takes in a noisy optimized point \tilde{z} and projects it back onto or near the manifold.

To train Ψ , we adopt a denoising objective that projects noisy samples back towards the clean points on the latent manifold. Given a clean latent embedding z , we construct a short corruption chain $\tilde{z}^{(0)} = z$, $\tilde{z}^{(k)} \sim C(\tilde{Z} | \tilde{Z}^{(k-1)}, \sigma_k)$, $k = 1, \dots, K$, where $C(\cdot, \sigma_k)$ denotes Gaussian corruption with noise level σ_k . The projector is trained to reverse each step by predicting $\tilde{z}^{(k-1)}$ from $\tilde{z}^{(k)}$, yielding the objective in equation 2.

$$\mathcal{L}_{\Psi} = \mathbb{E}_{z \sim p_{\text{data}}} \sum_{k=1}^K \mathbb{E}_{\tilde{z}^{(k)} \sim C(\cdot | \tilde{z}^{(k-1)}, \sigma_k)} \left[\|\Psi(\tilde{z}^{(k)}) - \tilde{z}^{(k-1)}\|_2^2 \right] \quad (2)$$

When $K = 1$, this reduces to the standard denoising autoencoder loss (Vincent et al., 2008). We keep K small (e.g. 1 to 3) to capture *local updates near the data manifold*, rather than simulating long diffusion chains from Gaussian noise. As a result, our algorithm is fast during training and inference.

3.3. Property-guided manifold Langevin dynamics

Next, we introduce a novel property-guided manifold Langevin-dynamics framework.

Given a trained encoder \mathcal{E} , a property predictor \mathcal{P} , and a manifold projector Ψ , our Langevin-dynamics framework optimizes sequences for a target property. Starting from the latent embedding $z = \mathcal{E}(x)$ of a sequence x , we iteratively update it using a gradient-based drift term $\nabla_z f(z)$, inject Gaussian noise ϵ , and apply a manifold projector $\Psi(\cdot)$ to ensure biological viability and interpretability. We define the update rule as described in equation 3.

$$\begin{aligned} z_{t+1} &= \Psi(z_t + dz_t) \\ dz_t &= \frac{\eta}{\tau} \nabla_z f(z_t) + \sqrt{2\eta} \epsilon_t, \quad \epsilon_t \sim \mathcal{N}(0, I) \end{aligned} \quad (3)$$

Here, η is the step size, τ is the temperature hyperparameter,

and $\nabla_z f(z)$ denotes the property gradient given by the predictor \mathcal{P} . A smaller τ emphasizes focused updates along the gradient, while a larger τ encourages more diverse exploration. When $\tau \rightarrow \infty$, the property guidance vanishes and the update rule is dominated by the stochastic term, which becomes similar to generative modeling with the walkback algorithm (Bengio et al., 2013).

The manifold projector Ψ , analogous to the retraction in Riemannian SGD (Bonnabel, 2013), is applied after each update to ensure that each step remains near the biologically valid latent manifold, enabling interpretable and controllable generation trajectories.

With the trained components \mathcal{E} , \mathcal{P} and Ψ , we can optimize the target property of any given sequence. Notably, optimization entails both maximization and minimization: users can choose to increase or decrease the target property, depending on the application.

4. Empirical Results

We evaluate RNAGenScape on property-optimized mRNA sequence generation across multiple biologically relevant settings. The goal is to improve target properties such as translation efficiency and stability while preserving the biological viability of the generated sequences. To this end, we conducted comprehensive experiments to analyze the property gains, biological viability, efficiency, and optimization trajectories.

4.1. Experimental settings

Datasets and the properties to optimize We evaluated RNAGenScape on three mRNA datasets that capture diverse contexts and experimental designs. The optimization objectives are underlined.

1. `OpenVaccine` contains 2,400 mRNA sequences devised for COVID-19 mRNA vaccines, each with 107 nucleotides (Das et al., 2020). The target property is mRNA stability, which is directly relevant to vaccine performance.
2. `Zebrafish` consists of five subsets of zebrafish 5' UTR mRNA sequences each with 124 nucleotides, comprising approximately 55,000 sequences in total. The target property is translation efficiency, which measures how effectively an mRNA sequence is translated into protein.
3. `Ribosome` is a large-scale dataset of approximately 260,000 5' UTR mRNA sequences, each with 50 nucleotides (Sample et al., 2019). The target property is the mean ribosome load, defined as the average number of ribosomes bound to the mRNA during translation.

Table 1. Our proposed RNAGenScape generates biologically viable mRNA sequences that achieve superior property optimization. In property optimization results, Δ denotes the median change in property and % denotes success rate (percentage of mRNAs improved). In the biological viability checks, uORF OOF AUG denote out-of-frame start codon in the upstream open reading frame, and Kozak similarity is the similarity to the consensus Kozak sequence. The best values per metric are highlighted in bold.

Method	Property Optimization				Biological Viability Checks			
	+Property		-Property		Initiation Interference		Initiation Context	Structural Stability
	$\Delta \uparrow$	% \uparrow	$\Delta \downarrow$	% \uparrow	uORF	OOF AUG % \downarrow	Kozak Similarity % \uparrow	Minimum Free Energy \downarrow
<i>OpenVaccine (n\approx2k), property to optimize: stability</i>								
Data in the test set	—	—	—	—	1.65 \pm 0.23	37.90 \pm 30.38	-30.13 \pm 17.76	
DiffAb (Luo et al., 2022)	+0.06	55.0	+0.11	44.0	1.75 \pm 2.29	27.79 \pm 30.03	-21.10 \pm 12.46	
IgLM (Shuai et al., 2023)	+0.24	63.1	+0.01	49.6	1.24 \pm 1.76	21.12 \pm 28.62	-4.59 \pm 3.87	
NOS-C (Gruver et al., 2023)	+0.09	54.6	-2.25	90.6	1.71 \pm 2.29	3.85 \pm 10.72	-0.26 \pm 0.83	
NOS-D (Gruver et al., 2023)	+0.18	58.3	-0.29	65.4	2.27 \pm 2.52	32.40 \pm 30.06	-18.81 \pm 5.82	
RNAGenScape (ours)	+0.54	77.5	-2.81	97.9	1.63 \pm 0.59	34.65 \pm 23.26	-25.78 \pm 3.17	
<i>Gain over baselines</i>	+125%	+22.8%	+24.9%	+8.1%	—	—	—	
<i>Zebrafish (n\approx55k), property to optimize: translation efficiency</i>								
Data in the test set	—	—	—	—	2.51 \pm 2.65	33.92 \pm 29.42	-29.40 \pm 7.20	
DiffAb (Luo et al., 2022)	-0.21	36.3	-0.21	60.8	3.75 \pm 2.65	23.84 \pm 29.41	-27.31 \pm 7.19	
IgLM (Shuai et al., 2023)	-0.57	32.0	-0.83	74.3	2.90 \pm 2.07	22.38 \pm 28.15	-6.30 \pm 3.16	
NOS-C (Gruver et al., 2023)	+0.03	51.1	-1.07	80.8	2.70 \pm 1.56	20.77 \pm 18.50	-0.09 \pm 0.39	
NOS-D (Gruver et al., 2023)	+0.31	57.5	+0.38	40.2	2.43 \pm 1.59	18.01 \pm 20.02	-2.28 \pm 2.42	
RNAGenScape (ours)	+0.77	75.0	-1.29	85.1	2.41 \pm 1.98	26.17 \pm 17.43	-29.24 \pm 6.17	
<i>Gain over baselines</i>	+148%	+30.4%	+20.6%	+5.3%	—	—	—	
<i>Ribosome (n\approx260k), property to optimize: mean ribosome load</i>								
Data in the test set	—	—	—	—	3.32 \pm 4.25	20.60 \pm 29.54	-8.65 \pm 3.66	
DiffAb (Luo et al., 2022)	-0.05	45.0	-0.04	54.2	3.16 \pm 4.19	14.68 \pm 28.77	-7.25 \pm 3.57	
IgLM (Shuai et al., 2023)	+0.63	80.5	-0.51	65.5	6.14 \pm 4.85	7.73 \pm 20.51	-7.27 \pm 3.38	
NOS-C (Gruver et al., 2023)	+0.08	53.6	+0.10	46.0	4.53 \pm 3.89	12.96 \pm 22.88	-5.79 \pm 2.98	
NOS-D (Gruver et al., 2023)	-0.09	46.5	-0.10	53.6	5.64 \pm 5.06	8.05 \pm 16.27	-0.77 \pm 1.35	
RNAGenScape (ours)	+0.63	81.4	-0.58	67.8	4.51 \pm 3.68	16.41 \pm 28.42	-8.23 \pm 3.18	
<i>Gain over baselines</i>	+0.0%	+1.1%	+13.7%	+3.5%	—	—	—	

Reproducibility All experiments were repeated using 5 random seeds and the average results are reported. Details are summarized in Supplementary Section A.

4.2. RNAGenScape generates biologically viable, property-optimized mRNA sequences

Across all three datasets, we evaluate RNAGenScape along two complementary axes: improvement of the target property and preservation of biological viability. Both aspects are jointly reported in Table 1.

Property optimization is assessed using UTR-LM (Chu et al., 2024), a widely adopted mRNA language model, as the external oracle. UTR-LM is first pre-trained on over 480,000 5' UTR sequences from diverse sources and subsequently fine-tuned for property prediction on each dataset. After fine-tuning, the model is frozen and never accessed during optimization, ensuring an unbiased evaluation of the optimized sequences.

To assess biological viability, we apply a set of complementary checks grounded in established principles of mRNA translation. Specifically, we consider three classes of viability metrics. First, upstream out-of-frame start codons

(uORF OOF AUG) are known to suppress downstream protein expression and are therefore undesirable (Dever et al., 2023). Second, Kozak similarity (Gleason et al., 2022) measures how closely the initiation context matches the consensus Kozak sequence, with higher values indicating more favorable translation initiation. Third, minimum free energy (Lorenz et al., 2011) serves as a proxy for mRNA structural stability.

Across all three datasets and both optimization directions, RNAGenScape achieves the largest median property change and the highest success rate (Table 1). Compared to state-of-the-art biological sequence optimization methods, including DiffAb (Luo et al., 2022), IgLM (Shuai et al., 2023), NOS-C (Gruver et al., 2023), and NOS-D (Gruver et al., 2023), RNAGenScape attains up to a 148% increase in median property improvement and up to a 30% increase in success rate. In addition to better optimization performance, RNAGenScape consistently produces sequences with fewer aberrant upstream start codons, higher Kozak similarity, and more favorable minimum free energy profiles. Moreover, the viability metrics of RNAGenScape-generated sequences more closely match those of real sequences in the unseen test set,

indicating that substantial property gains can be achieved without compromising biological viability.

4.3. Held-out validation on unseen near-optimal sequences

Table 2. Edit distance between each generated sequence and its nearest held-out sequence with near-optimal property. Edit distance is normalized to $[0, 1]$, with lower values being better.

	DiffAb (Luo et al., 2022)	IgLM (Shuai et al., 2023)	NOS-C (Gruver et al., 2023)	NOS-D (Gruver et al., 2023)	RNAGenScope (ours)
OpenVaccine ($n \approx 2k$)	0.434 ± 0.086	0.533 ± 0.045	0.651 ± 0.037	0.543 ± 0.031	0.356 ± 0.025
Zebrafish ($n \approx 55k$)	0.658 ± 0.076	0.690 ± 0.020	0.826 ± 0.021	0.783 ± 0.023	0.484 ± 0.014
Ribosome ($n \approx 260k$)	0.418 ± 0.193	0.503 ± 0.024	0.526 ± 0.026	0.652 ± 0.032	0.262 ± 0.134

To further assess whether RNAGenScope produces realistic property-optimized solutions, we conducted a held-out validation designed to mimic a practical design scenario. Specifically, for each dataset, we withheld a subset of sequences that already exhibit near-optimal target properties and excluded them from optimization. The property threshold is set at one standard deviation better than the mean. We then evaluate how close the generated sequences are to these held-out high-quality references.

Table 2 reports the normalized edit distance between each generated sequence and its nearest held-out sequence with a near-optimal property. Across all datasets, RNAGenScope consistently achieves the lowest edit distance compared to alternative biological sequence generation methods, indicating that it converges to realistic, high-performing sequences. These results suggest that RNAGenScope not only improves target properties, but does so in a manner that recovers solutions closely aligned with experimentally observed sequences.

4.4. Efficiency and scalability

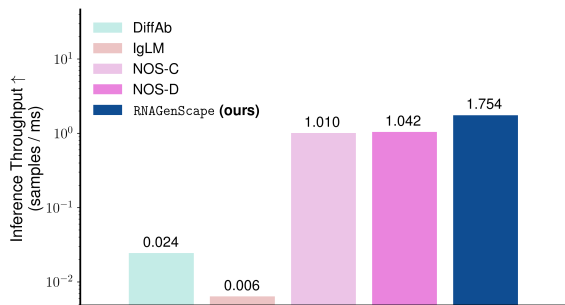


Figure 2. Inference throughput of all optimization methods.

In addition to its other merits, RNAGenScope is also highly efficient at inference time. As reported in Figure 2, it achieves a throughput of 1.754 sample/ms, 68% faster than the most efficient biological sequence optimization method being compared. This efficiency makes RNAGenScope

well suited for large-scale or iterative design workflows where high throughput is essential.

4.5. Ablation studies

Table 3. Reconstruction and prediction objectives in organized autoencoder are constructive and complementary.

	$\mathcal{L}_{\text{Recon}}$	$\mathcal{L}_{\text{Pred}}$	Reconstruction		Property Prediction	
			Nucleotide Acc. \uparrow	Pearson Corr. \uparrow	Spearman Corr. \uparrow	
OpenVaccine ($n \approx 2k$)	\checkmark	\times	0.49	-0.08	-0.08	
	\times	\checkmark	0.17	0.75	0.75	
	\checkmark	\checkmark	0.67	0.70	0.71	
Zebrafish ($n \approx 55k$)	\checkmark	\times	0.80	-0.04	-0.03	
	\times	\checkmark	0.17	0.54	0.60	
	\checkmark	\checkmark	0.78	0.63	0.67	
Ribosome ($n \approx 260k$)	\checkmark	\times	0.99	-0.08	-0.15	
	\times	\checkmark	0.11	0.87	0.85	
	\checkmark	\checkmark	0.99	0.87	0.85	

Table 4. The manifold projector Ψ substantially improves property optimization by enforcing optimization along the data manifold.

	Ψ	+property		-property	
		$\Delta \uparrow$	% \uparrow	$\Delta \downarrow$	% \uparrow
OpenVaccine ($n \approx 2k$)	\times	-0.44	33.3	-0.49	66.5
	\checkmark	0.54	77.5	-2.81	97.9
Zebrafish ($n \approx 55k$)	\times	0.15	54.7	-0.83	71.9
	\checkmark	0.77	75.0	-1.29	85.1
Ribosome ($n \approx 260k$)	\times	-0.17	45.1	0.13	47.0
	\checkmark	0.63	81.4	-0.58	67.8

Organized autoencoder Since the optimization process in RNAGenScope is performed in the learned latent manifold, we verify that the OAE provides both accurate reconstruction and property prediction (Table 3). Additionally, we demonstrate that the reconstruction and prediction objectives ($\mathcal{L}_{\text{Recon}}$ and $\mathcal{L}_{\text{Pred}}$) are constructive to each other, which justifies our OAE design.

Manifold projector Next, we show that the manifold projector Ψ is essential for the optimization performance of RNAGenScope (Table 4). Without Ψ , optimization becomes substantially less effective across datasets. This behavior is expected: updating latent representations solely by following the property gradient allows trajectories to drift away from the learned data manifold, entering regions that are weakly supported by real sequences. In these off-manifold regions, property gradients become less reliable, leading to unstable updates and diminished optimization gains.

Optimization steps We further analyze how sensitive RNAGenScope is to the number of optimization steps. The results in Figure 3 show that our method is able to converge quickly and remains stable over a range of optimization steps during Langevin dynamics updates.

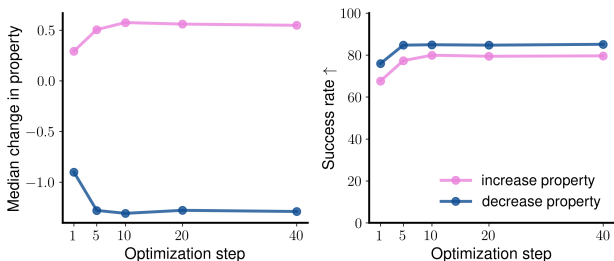


Figure 3. RNAGenScope optimization is step-efficient and remains stable over a range of optimization steps.

Table 5. RNAGenScope achieves better property optimization than *de novo* generative methods and classic optimization algorithms that operate on our learned data manifold.

Method	Property Optimization			
	+Property		-Property	
	$\Delta \uparrow$	% \uparrow	$\Delta \downarrow$	% \uparrow
OpenVaccine (n≈2k)				
VAE (Kingma et al., 2013)	-0.23	42.1	-0.23	57.9
DDPM (Ho et al., 2020)	-0.33	33.8	-0.33	66.2
LDM (Rombach et al., 2022)	-0.07	47.5	-0.07	52.5
FM (Lipman et al., 2022)	-0.34	32.5	-0.34	67.5
OAE + gradient ascent	-0.01	51.0	-0.19	61.3
OAE + MCMC	-0.11	45.1	-0.19	57.7
OAE + hill climbing	+0.40	69.2	-0.29	64.2
OAE + stochastic hill climbing	-0.12	43.5	-0.15	60.0
RNAGenScope (ours)	+0.54	77.5	-2.81	97.9
Zebrafish (n≈55k)				
VAE (Kingma et al., 2013)	-0.01	49.4	-0.01	50.6
DDPM (Ho et al., 2020)	+0.29	58.2	+0.29	41.8
LDM (Rombach et al., 2022)	-0.95	22.5	-0.95	77.5
FM (Lipman et al., 2022)	+0.32	59.8	+0.32	40.2
OAE + gradient ascent	-0.21	18.0	-0.33	66.5
OAE + MCMC	-0.20	44.3	-0.37	60.1
OAE + hill climbing	+0.76	74.4	-0.87	75.2
OAE + stochastic hill climbing	+0.32	60.3	-0.80	73.7
RNAGenScope (ours)	+0.77	75.0	-1.29	85.1
Ribosome (n≈260k)				
VAE (Kingma et al., 2013)	-0.24	41.7	-0.24	58.3
DDPM (Ho et al., 2020)	-0.11	45.9	-0.11	54.1
LDM (Rombach et al., 2022)	-0.24	41.8	-0.24	58.2
FM (Lipman et al., 2022)	-0.10	46.4	-0.10	53.6
OAE + gradient ascent	+0.43	73.6	-0.05	55.7
OAE + MCMC	-0.19	43.0	-0.10	54.2
OAE + hill climbing	+0.53	83.0	-0.06	56.1
OAE + stochastic hill climbing	+0.19	60.4	-0.05	55.2
RNAGenScope (ours)	+0.63	81.4	-0.58	67.8

De novo generative methods and classic optimization algorithms In addition to state-of-the-art biological sequence optimization methods, we compare RNAGenScope with two different types of methods. The first type is *de novo* generative modeling approaches,

namely variational autoencoder (VAE) (Kingma et al., 2013), denoising diffusion probabilistic model (DDPM) (Ho et al., 2020), latent diffusion model (LDM) (Rombach et al., 2022), and flow matching (FM) (Lipman et al., 2022). The second type are classic optimization algorithms that operate in our OAE latent manifold, including gradient ascent (Williams, 1992; Zinkevich, 2003), Markov chain Monte Carlo (MCMC) (Brooks, 1998; Andrieu et al., 2003), and hill climbing (Selman & Gomes, 2006). All classic optimization baselines are GPU-compatible re-implementations of Castro et al. (Castro et al., 2022).

The results in Table 5 show that 1) *de novo* generative models exhibit limited property control and 2) classic optimization strategies in the OAE latent manifold also underperform RNAGenScope, indicating that our manifold Langevin dynamics contributed substantially to the favorable performance. See Figure S1 for the optimization performance of all methods being compared.

4.6. Case study: RNAGenScope produces structured, data-aligned optimization trajectories

To illustrate how RNAGenScope iteratively navigates along a learned latent manifold, we visualize a sample optimization run in Figure 4a. The trajectory exhibits monotonic increases in the target property, while remaining near regions populated by real sequences. See Supplementary Section E for more examples. These trajectories are direct consequences of the manifold-constrained dynamics, which guided each step toward high-property regions while staying on the manifold.

As a qualitative illustration of biological plausibility, we show that the intermediate results of RNAGenScope optimization can be properly folded by RhoFold (Shen et al., 2024) into 3D structures (Figure 4b). In contrast, folding intermediate products of several other methods causes failure, as indicated by fragmented structures (Figure 4b).

5. Related Works

Table 6. Characteristics of the models: whether they can perform (1) generation, (2) optimization, (3) interpolation, and (4) whether they produce optimization trajectories.

Method	Gen.	Opt.	Interp.	Traj.
<i>de novo</i> generative models	✓	✗/✓	✗	✗
classic optimization methods	✗/✓	✓	✗	✓
DiffAb (Luo et al., 2022)	✓	✓	✗	✓
IgLM (Shuai et al., 2023)	✓	✓	✗	✗
NOS (Gruver et al., 2023)	✓	✓	✗	✗
RNAGenScope (ours)	✓	✓	✓	✓

Machine learning is becoming increasingly popular for optimizing biological sequences such as DNA, RNA, and

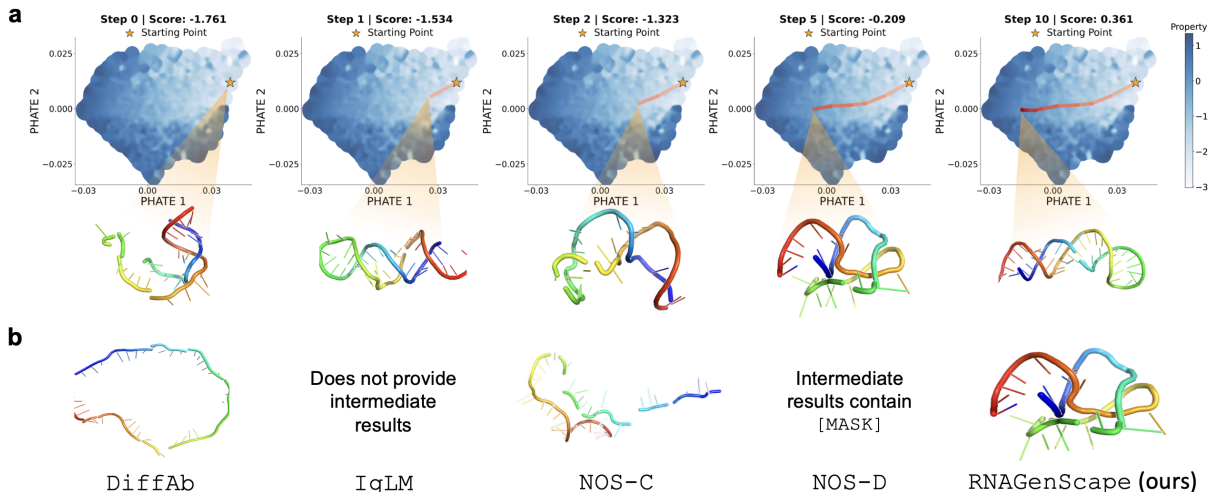


Figure 4. A sample latent space trajectory of RNAGenScape over 10 optimization steps. The trajectory follows a smooth path with steady improvement in the target property. **a**, The trajectory in the PHATE space and the corresponding 3D structures. **b**, Intermediate results of RNAGenScape and competing methods midway through property optimization (at the 5th step out of 10 steps).

proteins. This section reviews recent advances in sequence modeling and optimization, with an emphasis on mRNAs.

Current machine learning approaches for sequence design can be grouped into three main paradigms, but each addresses only part of the challenge (Table 6).

De novo generative models excel at creating novel sequences, but fundamentally operate by generating from scratch rather than refining existing functional sequences (Prykhodko et al., 2019; Méndez-Lucio et al., 2020; Dauparas et al., 2022; Wu et al., 2021; Madani et al., 2023; Watson et al., 2023). Classic optimization strategies (Williams, 1992; Zinkevich, 2003; Brooks, 1998; Andrieu et al., 2003; Selman & Gomes, 2006) are capable of improving known sequences, but typically lack mechanisms to ensure that intermediate variants remain consistent with the underlying biological distribution. More recent deep learning methods for sequence generation and optimization (Luo et al., 2022; Shuai et al., 2023; Gruver et al., 2023) aim to combine generative modeling with property-driven objectives, but their optimization trajectories remain opaque, offering limited interpretability of which sequence changes drive functional improvements. Furthermore, existing methods cannot interpolate between sequences. Consequently, a framework that enables biologically-grounded sequence engineering remains needed (Wu et al., 2019).

An extended related works section can be found in Supplementary Section F.

6. Conclusion

We introduced RNAGenScape, a manifold Langevin dynamics framework for property-optimized mRNA

sequence generation. Rather than optimizing in the ambient sequence space, RNAGenScape operates directly on a learned manifold of viable mRNA sequences. In this setting, property gradients are more reliable, biological viability is better preserved, and optimization can be performed with lower computational overhead. Comprehensive experiments on three real-world mRNA datasets show that our method leads to greater property gains and higher success rates under realistic data regimes. With this work, we aim to shift the paradigm of biological sequence design from unconstrained generation toward guided optimization, and to highlight mRNA sequence design as a critical yet understudied frontier in computational biology.

7. Limitations and Future Work

One limitation of RNAGenScape is that it exclusively models and optimizes mRNA sequences only, without explicitly incorporating mRNA structure. While sequence-based representations capture many aspects of mRNA function, structures can provide auxiliary information in regulating translation, stability, and interactions.

In future work, we will study the possibility of performing sequence-structure joint modeling and optimization. Beyond mRNA, we plan to extend RNAGenScape to other modalities such as protein sequences and regulatory elements, and integrate active learning frameworks that guide wet lab experimentation. By grounding sequence optimization in the manifold of real data, we aim to provide a versatile platform for interpretable high-throughput design in synthetic biology.

Impact Statement

This work proposes a machine learning framework for optimizing mRNA sequences while preserving biological viability by constraining optimization to a learned data manifold. Potential positive impacts include supporting computational design workflows in mRNA therapeutics and synthetic biology such as vaccine development by enabling more controlled and interpretable sequence refinement. As a general machine learning contribution, the framework may also inform broader research on manifold-constrained optimization for biological sequences.

The approach is intended as a computational tool to complement experimental and domain expertise rather than a substitute for empirical validation. As with other data-driven sequence models, limitations and biases in the available training data may influence optimization outcomes, and inappropriate use without biological oversight could lead to nonfunctional or misleading designs.

We do not anticipate direct negative societal consequences arising from this work beyond those already associated with machine learning-based biological modeling. We encourage future research to further study robustness, data bias, and safe integration of such methods into experimental pipelines.

References

- Afrasiyabi, A., Kovalic, J., Liu, C., Castro, E., Weinreb, A., Varol, E., Miller, D., Hammarlund, M., and Krishnaswamy, S. Cellsplicenet: Interpretable multimodal modeling of alternative splicing across neurons in *c. elegans*. *bioRxiv*, pp. 2025–06, 2025.
- Andrieu, C., De Freitas, N., Doucet, A., and Jordan, M. I. An introduction to mcmc for machine learning. *Machine learning*, 50:5–43, 2003.
- Asim, M. N., Ibrahim, M. A., Asif, T., and Dengel, A. Rna sequence analysis landscape: A comprehensive review of task types, databases, datasets, word embedding methods, and language models. *Heliyon*, 11(2), 2025.
- Bengio, Y., Yao, L., Alain, G., and Vincent, P. Generalized denoising auto-encoders as generative models, 2013. URL <https://arxiv.org/abs/1305.6663>.
- Bonnabel, S. Stochastic gradient descent on riemannian manifolds. *IEEE Transactions on Automatic Control*, 58(9):2217–2229, September 2013. ISSN 1558-2523. doi: 10.1109/tac.2013.2254619. URL <http://dx.doi.org/10.1109/TAC.2013.2254619>.
- Brooks, S. Markov chain monte carlo method and its application. *Journal of the royal statistical society: series D (the Statistician)*, 47(1):69–100, 1998.
- Burkhardt, D. B., Stanley III, J. S., Tong, A., Perdigoto, A. L., Gigante, S. A., Herold, K. C., Wolf, G., Giraldez, A. J., van Dijk, D., and Krishnaswamy, S. Quantifying the effect of experimental perturbations at single-cell resolution. *Nature biotechnology*, 39(5):619–629, 2021.
- Calvanese, F., Lambert, C. N., Nghe, P., Zamponi, F., and Weigt, M. Towards parsimonious generative modeling of rna families. *Nucleic Acids Research*, 52(10):5465–5477, 2024.
- Castillo-Hair, S., Fedak, S., Wang, B., Linder, J., Havens, K., Certo, M., and Seelig, G. Optimizing 5’utrs for mrna-delivered gene editing using deep learning. *Nature Communications*, 15(1):5284, 2024.
- Castillo-Hair, S. M. and Seelig, G. Machine learning for designing next-generation mrna therapeutics. *Accounts of chemical research*, 55(1):24–34, 2021.
- Castro, E., Godavarthi, A., Rubinfien, J., Givechian, K., Bhaskar, D., and Krishnaswamy, S. Transformer-based protein generation with regularized latent space optimization. *Nature Machine Intelligence*, 4(10):840–851, 2022.
- Cayton, L. et al. *Algorithms for manifold learning*. eScholarship, University of California, 2008.
- Chaudhary, N., Weissman, D., and Whitehead, K. A. mrna vaccines for infectious diseases: principles, delivery and clinical translation. *Nature reviews Drug discovery*, 20(11):817–838, 2021.
- Chen, Y., Du, Z., Ren, X., Pan, C., Zhu, Y., Li, Z., Meng, T., and Yao, X. mrna-cla: An interpretable deep learning approach for predicting mrna subcellular localization. *Methods*, 227:17–26, 2024.
- Chu, Y., Yu, D., Li, Y., Huang, K., Shen, Y., Cong, L., Zhang, J., and Wang, M. A 5’utr language model for decoding untranslated regions of mrna and function predictions. *Nature Machine Intelligence*, 6(4):449–460, 2024.
- Das, R., Wayment-Steele, H., Do Soon Kim, C. C., Tunguz, B., Reade, W., and Demkin, M. Openvaccine: Covid-19 mrna vaccine degradation prediction, 2020. URL <https://kaggle.com/competitions/stanford-covid-vaccine>, 2020.
- Dauparas, J., Anishchenko, I., Bennett, N., Bai, H., Ragotte, R. J., Milles, L. F., Wicky, B. I., Courbet, A., de Haas, R. J., Bethel, N., et al. Robust deep learning-based protein sequence design using proteinmpnn. *Science*, 378(6615):49–56, 2022.

- Dever, T. E., Ivanov, I. P., and Hinnebusch, A. G. Translational regulation by uorfs and start codon selection stringency. *Genes & development*, 37(11-12):474–489, 2023.
- Eastman, P., Shi, J., Ramsundar, B., and Pande, V. S. Solving the rna design problem with reinforcement learning. *PLoS computational biology*, 14(6):e1006176, 2018.
- Fefferman, C., Mitter, S., and Narayanan, H. Testing the manifold hypothesis. *Journal of the American Mathematical Society*, 29(4):983–1049, 2016.
- Givechian, K. B., Rocha, J. F., Liu, C., Yang, E., Tyagi, S., Greene, K., Ying, R., Caron, E., Iwasaki, A., and Krishnaswamy, S. Immunostruct enables multimodal deep learning for immunogenicity prediction. *Nature Machine Intelligence*, pp. 1–14, 2025.
- Gleason, A. C., Ghadge, G., Chen, J., Sonobe, Y., and Roos, R. P. Machine learning predicts translation initiation sites in neurologic diseases with nucleotide repeat expansions. *PLoS One*, 17(6):e0256411, 2022.
- Goodfellow, I., Pouget-Abadie, J., Mirza, M., Xu, B., Warde-Farley, D., Ozair, S., Courville, A., and Bengio, Y. Generative adversarial networks. *Communications of the ACM*, 63(11):139–144, 2020.
- Gruver, N., Stanton, S., Frey, N., Rudner, T. G., Hotzel, I., Lafrance-Vanasse, J., Rajpal, A., Cho, K., and Wilson, A. G. Protein design with guided discrete diffusion. *Advances in neural information processing systems*, 36: 12489–12517, 2023.
- He, S., Gao, B., Sabnis, R., and Sun, Q. Rnadegformer: accurate prediction of mrna degradation at nucleotide resolution with deep learning. *Briefings in Bioinformatics*, 24(1):bbac581, 2023a.
- He, Y., Murata, N., Lai, C.-H., Takida, Y., Uesaka, T., Kim, D., Liao, W.-H., Mitsufuji, Y., Kolter, J. Z., Salakhutdinov, R., et al. Manifold preserving guided diffusion. *arXiv preprint arXiv:2311.16424*, 2023b.
- Hinton, G. E. and Salakhutdinov, R. R. Reducing the dimensionality of data with neural networks. *science*, 313(5786):504–507, 2006.
- Ho, J., Jain, A., and Abbeel, P. Denoising diffusion probabilistic models. *Advances in neural information processing systems*, 33:6840–6851, 2020.
- Kidger, P., Foster, J., Li, X., and Lyons, T. J. Neural sdes as infinite-dimensional gans. In *International conference on machine learning*, pp. 5453–5463. PMLR, 2021.
- Kingma, D. P., Welling, M., et al. Auto-encoding variational bayes, 2013.
- Li, Q., Hu, Y., Liu, Y., Zhang, D., Jin, X., and Chen, Y. Discrete point-wise attack is not enough: Generalized manifold adversarial attack for face recognition. In *Proceedings of the IEEE/CVF conference on computer vision and pattern recognition*, pp. 20575–20584, 2023.
- Li, T. and He, K. Back to basics: Let denoising generative models denoise. *arXiv preprint arXiv:2511.13720*, 2025.
- Li, T., Liu, G., Bu, G., Xu, Y., He, C., and Zhao, G. Optimizing mrna translation efficiency through rational 5’ utr and 3’ utr combinatorial design. *Gene*, 942:149254, 2025.
- Liao, D., Liu, C., Christensen, B. W., Tong, A., Huguet, G., Wolf, G., Nickel, M., Adelstein, I., and Krishnaswamy, S. Assessing neural network representations during training using noise-resilient diffusion spectral entropy. In *2024 58th Annual Conference on Information Sciences and Systems (CISS)*, pp. 1–6. IEEE, 2024.
- Licalatosi, D. D. and Darnell, R. B. Resolving rna complexity to decipher regulatory rules governing biological networks. *Nature Reviews. Genetics*, 11(1):75, 2010.
- Lindenbaum, O., III, J. S. S., Wolf, G., and Krishnaswamy, S. Geometry-based data generation, 2018. URL <https://arxiv.org/abs/1802.04927>.
- Linder, J. and Seelig, G. Fast activation maximization for molecular sequence design. *BMC bioinformatics*, 22: 1–20, 2021.
- Linder, J., Bogard, N., Rosenberg, A. B., and Seelig, G. Deep exploration networks for rapid engineering of functional dna sequences. *BioRxiv*, pp. 864363, 2019.
- Lipman, Y., Chen, R. T., Ben-Hamu, H., Nickel, M., and Le, M. Flow matching for generative modeling. *arXiv preprint arXiv:2210.02747*, 2022.
- Liu, C., Amodio, M., Shen, L. L., Gao, F., Avesta, A., Aneja, S., Wang, J. C., Del Priore, L. V., and Krishnaswamy, S. CUTS: A Deep Learning and Topological Framework for Multigranular Unsupervised Medical Image Segmentation. In *proceedings of Medical Image Computing and Computer Assisted Intervention – MICCAI 2024*, volume LNCS 15008. Springer Nature Switzerland, October 2024.
- Liu, C., Liao, D., Parada-Mayorga, A., Ribeiro, A., DiStasio, M., and Krishnaswamy, S. Diffkillr: Killing and recreating diffeomorphisms for cell annotation in dense microscopy images. In *ICASSP 2025-2025 IEEE*

- International Conference on Acoustics, Speech and Signal Processing (ICASSP)*. IEEE, 2025a.
- Liu, C., Xu, K., Shen, L. L., Huguét, G., Wang, Z., Tong, A., Bzdok, D., Stewart, J., Wang, J. C., Del Priore, L. V., and Krishnaswamy, S. Imageflownet: Forecasting multiscale trajectories of disease progression with irregularly-sampled longitudinal medical images. In *ICASSP 2025-2025 IEEE International Conference on Acoustics, Speech and Signal Processing (ICASSP)*. IEEE, 2025b.
- Lorenz, R., Bernhart, S. H., Höner zu Siederdisen, C., Tafer, H., Flamm, C., Stadler, P. F., and Hofacker, I. L. Viennarna package 2.0. *Algorithms for molecular biology*, 6(1):26, 2011.
- Luo, S., Su, Y., Peng, X., Wang, S., Peng, J., and Ma, J. Antigen-specific antibody design and optimization with diffusion-based generative models for protein structures. *Advances in Neural Information Processing Systems*, 35: 9754–9767, 2022.
- Ma, Q., Zhang, X., Yang, J., Li, H., Hao, Y., and Feng, X. Optimization of the 5' untranslated region of mrna vaccines. *Scientific Reports*, 14(1):19845, 2024.
- Madani, A., Krause, B., Greene, E. R., Subramanian, S., Mohr, B. P., Holton, J. M., Olmos Jr, J. L., Xiong, C., Sun, Z. Z., Socher, R., et al. Large language models generate functional protein sequences across diverse families. *Nature biotechnology*, 41(8):1099–1106, 2023.
- Méndez-Lucio, O., Baillif, B., Clevert, D.-A., Rouquié, D., and Wichard, J. De novo generation of hit-like molecules from gene expression signatures using artificial intelligence. *Nature communications*, 11(1):10, 2020.
- Moon, K. R., van Dijk, D., Wang, Z., Gigante, S., Burkhardt, D. B., Chen, W. S., Yim, K., Elzen, A. v. d., Hirn, M. J., Coifman, R. R., et al. Visualizing structure and transitions in high-dimensional biological data. *Nature biotechnology*, 37(12):1482–1492, 2019.
- Narayanan, H. and Mitter, S. Sample complexity of testing the manifold hypothesis. *Advances in neural information processing systems*, 23, 2010.
- Oliver, S. G. From dna sequence to biological function. *Nature*, 379(6566):597–600, 1996.
- Pardi, N., Hogan, M. J., Porter, F. W., and Weissman, D. mrna vaccines—a new era in vaccinology. *Nature reviews Drug discovery*, 17(4):261–279, 2018.
- Prykhodko, O., Johansson, S. V., Kotsias, P.-C., Arús-Pous, J., Bjerrum, E. J., Engkvist, O., and Chen, H. A de novo molecular generation method using latent vector based generative adversarial network. *Journal of cheminformatics*, 11(1):74, 2019.
- Qin, S., Tang, X., Chen, Y., Chen, K., Fan, N., Xiao, W., Zheng, Q., Li, G., Teng, Y., Wu, M., et al. mrna-based therapeutics: powerful and versatile tools to combat diseases. *Signal transduction and targeted therapy*, 7(1):166, 2022.
- Rifai, S., Dauphin, Y. N., Vincent, P., Bengio, Y., and Muller, X. The manifold tangent classifier. *Advances in neural information processing systems*, 24, 2011.
- Rombach, R., Blattmann, A., Lorenz, D., Esser, P., and Ommer, B. High-resolution image synthesis with latent diffusion models. In *Proceedings of the IEEE/CVF conference on computer vision and pattern recognition*, pp. 10684–10695, 2022.
- Sample, P. J., Wang, B., Reid, D. W., Presnyak, V., McFadyen, I. J., Morris, D. R., and Seelig, G. Human 5' utr design and variant effect prediction from a massively parallel translation assay. *Nature biotechnology*, 37(7): 803–809, 2019.
- Schlusser, N., González, A., Pandey, M., and Zavolan, M. Current limitations in predicting mrna translation with deep learning models. *Genome Biology*, 25(1):227, 2024.
- Selman, B. and Gomes, C. P. Hill-climbing search. *Encyclopedia of cognitive science*, 81(333-335):10, 2006.
- Shen, T., Hu, Z., Sun, S., Liu, D., Wong, F., Wang, J., Chen, J., Wang, Y., Hong, L., Xiao, J., et al. Accurate rna 3d structure prediction using a language model-based deep learning approach. *Nature Methods*, 21(12):2287–2298, 2024.
- Shuai, R. W., Ruffolo, J. A., and Gray, J. J. Iglm: Infilling language modeling for antibody sequence design. *Cell Systems*, 14(11):979–989, 2023.
- Sinai, S., Kelsic, E., Church, G. M., and Nowak, M. A. Variational auto-encoding of protein sequences. *arXiv preprint arXiv:1712.03346*, 2017.
- Song, Y. and Ermon, S. Generative modeling by estimating gradients of the data distribution. *Advances in neural information processing systems*, 32, 2019.
- Stanton, S., Maddox, W., Gruver, N., Maffettone, P., Delaney, E., Greenside, P., and Wilson, A. G. Accelerating bayesian optimization for biological sequence design with denoising autoencoders. In *International conference on machine learning*, pp. 20459–20478. PMLR, 2022.
- Sun, X., Liao, D., MacDonald, K., Zhang, Y., Liu, C., Huguét, G., Wolf, G., Adelstein, I., Rudner, T. G., and Krishnaswamy, S. Geometry-aware generative autoencoders for warped riemannian metric learning and

- generative modeling on data manifolds. In *International Conference on Artificial Intelligence and Statistics*. PMLR, 2025.
- Taubert, O., von der Lehr, F., Bazarova, A., Faber, C., Knechtges, P., Weiel, M., Debus, C., Coquelin, D., Basermann, A., Streit, A., et al. Rna contact prediction by data efficient deep learning. *Communications biology*, 6(1):913, 2023.
- Tong, A., Kuchroo, M., Gupta, S., Venkat, A., San Juan, B. P., Rangel, L., Zhu, B., Lock, J. G., Chaffer, C. L., and Krishnaswamy, S. Learning transcriptional and regulatory dynamics driving cancer cell plasticity using neural ode-based optimal transport. *bioRxiv*, pp. 2023–03, 2023.
- Vaishnav, E. D., de Boer, C. G., Molinet, J., Yassour, M., Fan, L., Adiconis, X., Thompson, D. A., Levin, J. Z., Cubillos, F. A., and Regev, A. The evolution, evolvability and engineering of gene regulatory dna. *Nature*, 603(7901):455–463, 2022.
- Van Dijk, D., Sharma, R., Nainys, J., Yim, K., Kathail, P., Carr, A. J., Burdziak, C., Moon, K. R., Chaffer, C. L., Pattabiraman, D., et al. Recovering gene interactions from single-cell data using data diffusion. *Cell*, 174(3):716–729, 2018.
- Vavilis, T., Stamoula, E., Ainatzoglou, A., Sachinidis, A., Lamprinou, M., Dardalas, I., and Vizirianakis, I. S. mrna in the context of protein replacement therapy. *Pharmaceutics*, 15(1):166, 2023.
- Vincent, P., Larochelle, H., Bengio, Y., and Manzagol, P.-A. Extracting and composing robust features with denoising autoencoders. In *Proceedings of the 25th international conference on Machine learning*, pp. 1096–1103, 2008.
- Watson, J. L., Juergens, D., Bennett, N. R., Trippe, B. L., Yim, J., Eisenach, H. E., Ahern, W., Borst, A. J., Ragotte, R. J., Milles, L. F., et al. De novo design of protein structure and function with rfdiffusion. *Nature*, 620(7976):1089–1100, 2023.
- Wayment-Steele, H. K., Kladwang, W., Strom, A. I., Lee, J., Treuille, A., Becka, A., Participants, E., and Das, R. Rna secondary structure packages evaluated and improved by high-throughput experiments. *Nature methods*, 19(10):1234–1242, 2022.
- Weinreb, C., Riesselman, A. J., Ingraham, J. B., Gross, T., Sander, C., and Marks, D. S. 3d rna and functional interactions from evolutionary couplings. *Cell*, 165(4):963–975, 2016.
- Williams, R. J. Simple statistical gradient-following algorithms for connectionist reinforcement learning. *Machine learning*, 8(3):229–256, 1992.
- Wirecki, T., Lach, G., Jaryani, F., Badepally, N. G., Moafinejad, S. N., Klaudel, G., and Bujnicki, J. M. Desirna: structure-based design of rna sequences with a monte carlo approach. *bioRxiv*, pp. 2023–06, 2023.
- Wu, Z., Kan, S. J., Lewis, R. D., Wittmann, B. J., and Arnold, F. H. Machine learning-assisted directed protein evolution with combinatorial libraries. *Proceedings of the National Academy of Sciences*, 116(18):8852–8858, 2019.
- Wu, Z., Johnston, K. E., Arnold, F. H., and Yang, K. K. Protein sequence design with deep generative models. *Current opinion in chemical biology*, 65:18–27, 2021.
- Yi, K., Zhou, B., Shen, Y., Liò, P., and Wang, Y. Graph denoising diffusion for inverse protein folding. *Advances in Neural Information Processing Systems*, 36:10238–10257, 2023.
- Zhang, H., Zhang, L., Lin, A., Xu, C., Li, Z., Liu, K., Liu, B., Ma, X., Zhao, F., Jiang, H., et al. Algorithm for optimized mrna design improves stability and immunogenicity. *Nature*, 621(7978):396–403, 2023.
- Zhang, Y., Huguet, G., De Brouwer, E., Liao, D., Fasina, O., Tong, A., Chen, R. T., Wolf, G., Nickel, M., Adelstein, I., et al. Neural fim: Bridging statistical manifolds and generative modeling through fisher geometry. *Authorea Preprints*, 2025.
- Zinkevich, M. Online convex programming and generalized infinitesimal gradient ascent. In *Proceedings of the 20th international conference on machine learning (icml-03)*, pp. 928–936, 2003.

Technical Appendices

A. Hyperparameters and Architecture

Learning the manifold with SUGAR To learn the manifold with SUGAR, we used the k -NN mode for estimating degrees (and thus sparsity) of latent points. We employed an α -decay kernel with $\alpha = 2$ and an adaptive bandwidth determined from the distance to the 5 nearest neighbors. The diffusion time was set to $t = 1$.

Training the organized autoencoder (OAE) We trained the OAE using the AdamW optimizer with an initial learning rate of 10^{-2} , together with a linear warmup cosine annealing scheduler. The learning rate was linearly increased from 10^{-4} (i.e., $0.01 \times$ the base learning rate) to the target value during the first 10% of training epochs (warmup), and then annealed to zero following a cosine decay schedule over the remaining epochs. We used a batch size of 128, a maximum of 200 epochs, and early stopping with a patience of 20 epochs based on the validation loss.

Training the manifold projector We trained the manifold projector Ψ using the AdamW optimizer with a learning rate of 10^{-4} . We used a batch size of 256, a maximum of 200 epochs, and applied early stopping with a patience of 20 epochs based on the validation loss.

Table S1. Hyperparameters used for different datasets.

Dataset	$\lambda_{\text{Recon}} / \lambda_{\text{Pred}}$	Noise levels	Langevin (step size, temperature)
Zebrafish	5.0 / 1.0	{1.0, 0.8, 0.5}	$1 \times 10^{-4}, 8 \times 2^{-4}$
OpenVaccine	1.0 / 1.0	{1.0, 0.5}	$1 \times 10^{-2}, 1 \times 10^{-2}$
Ribosome	1.0 / 1.0	{0.3}	$5 \times 10^{-3}, 1 \times 4^{-3}$

Organized Autoencoder (OAE) The organized autoencoder (OAE) maps mRNA sequences $x \in \mathbb{R}^{L \times V}$ to a compact latent $z \in \mathbb{R}^d$. Our latent dimension is 320 across all datasets.

For encoder, we apply three 1D convolutional blocks with GroupNorm, GELU, and channel squeeze-excitation (SE), followed by adaptive average pooling to length 8 and a linear projection. The property head is a three-layer MLP with GELU and dropout rate set to 0.3.

For decoding, a progressive 1D decoder upsamples structure gradually: we first expand z to a 128×8 seed map, then apply a stack of UpsampleBlock modules composed of upsampling and two residual convolutional blocks until reaching $\geq L$ positions; we then refine the output with two residue convolutional blocks to produce the final predicted logits. Weights are Kaiming/Xavier initialized; GroupNorm scales are set to 1 and biases to 0.

mRNA sequence vocabulary Although mRNA sequences naturally consist of the nucleotides A, U, G, and C, some experimental datasets represent U as T (borrowing the DNA alphabet). To handle this heterogeneity consistently, we define a unified vocabulary of size $V = 7$: <pad>, A, U, T, G, C, and N. Here, N denotes an unknown nucleotide during sequencing, and both U and T tokens are retained to ensure compatibility across datasets.

Hardware The evaluations were performed on a single NVIDIA A100 GPU. However, RNAGenScape can be run efficiently on more modest hardware.

B. Evaluation Metrics

Property Optimization To quantify the effectiveness of property optimization of different models, we measure both the median property gain and the fraction of sequences that are successfully optimized.

Specifically, given a test set of mRNA sequences X_{test} with predicted properties $\mathcal{P}_{\text{oracle}}(X_{\text{test}})$ and their optimized counterparts \tilde{X}_{test} with properties $\mathcal{P}_{\text{oracle}}(\tilde{X}_{\text{test}})$, we compute:

$$\Delta_{\text{median}} = \text{median}(\mathcal{P}_{\text{oracle}}(\tilde{x}) - \mathcal{P}_{\text{oracle}}(x)), \quad x \in X_{\text{test}}, \quad (4)$$

and

$$\%_{\text{success}} = \frac{1}{|X_{\text{test}}|} \sum_{x \in X_{\text{test}}} \mathbb{1}[\mathcal{P}_{\text{oracle}}(\tilde{x}) > \mathcal{P}_{\text{oracle}}(x)]. \quad (5)$$

Here, Δ_{median} measures the gain in the target property across the test set, while $\%_{\text{success}}$ reports the percentage of sequences that improve after optimization.

For models that cannot refine existing sequences (e.g., pure *de novo* generators), we assign a random pairing between initial and final sequences to enable a fair comparison.

The external oracle In our evaluation for property optimization, we use an external oracle $\mathcal{P}_{\text{oracle}}(x)$ to predict the property of sequences generated by RNAGenScape as well as competing methods. Specifically, we adopt UTR-LM (Chu et al., 2024), a widely used mRNA language model, as the property prediction oracle. It is first pre-trained on more than 480,000 5' UTR mRNA sequences from diverse sources, and then fine-tuned for property prediction on each of our datasets. After fine-tuning, it is frozen and never accessed during optimization, ensuring unbiased evaluation. Performance of the fine-tuned UTR-LM is shown in Table S2.

Table S2. The UTR-LM oracle for property evaluation.

	Property Prediction	
	Pearson Corr. \uparrow	Spearman Corr. \uparrow
OpenVaccine (n \approx 2k)	0.64	0.70
Zebrafish (n \approx 55k)	0.79	0.79
Ribosome (n \approx 260k)	0.91	0.89

C. Property optimization performance against all baselines

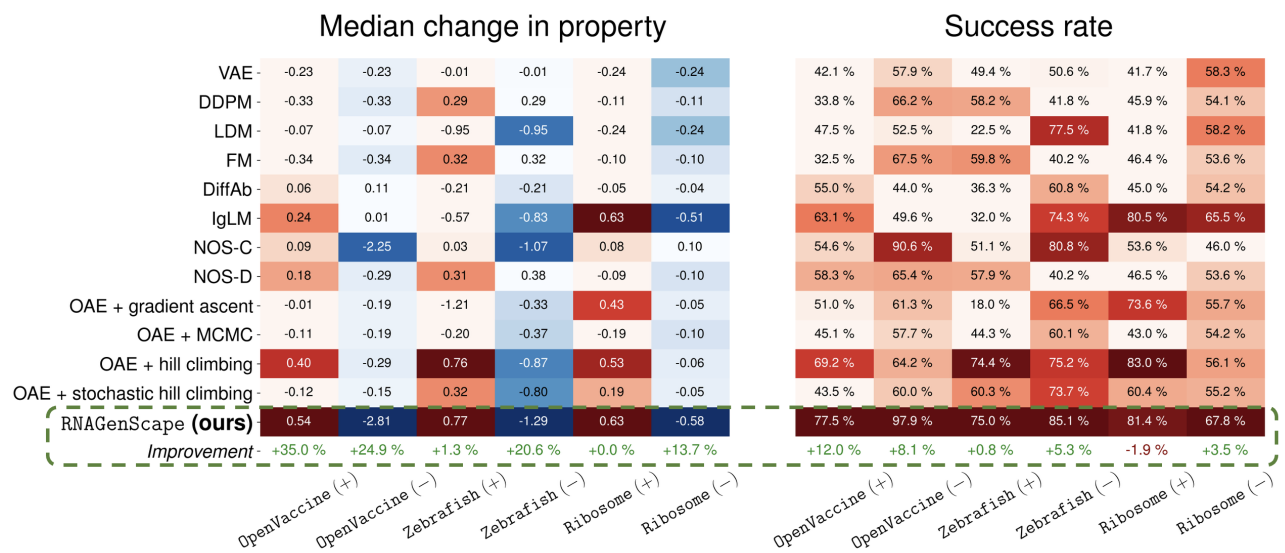


Figure S1. Quantitative comparison on property optimization. Median change in property (left) and success rate (right) are color-coded such that darker results are better. Properties of generated mRNA sequences are evaluated with the UTR-LM oracle pre-trained on more than 480,000 5' UTR mRNA sequences and fine-tuned on each of the three datasets. OpenVaccine ($n \approx 2k$, property: stability), Zebrafish ($n \approx 55k$, property: translation efficiency), and Ribosome ($n \approx 260k$, property: mean ribosome load).

D. Interpolation between sequences

In addition to optimizing mRNA sequences, we can interpolate between two existing sequences by guiding the latent embedding of one sequence toward that of another. Specifically, given a source sequence x_{source} and a target sequence x_{target} , we first obtain their latent embeddings via the encoder: $z_{\text{source}} = \mathcal{E}(x_{\text{source}})$ and $z_{\text{target}} = \mathcal{E}(x_{\text{target}})$.

We then perform property-guided Manifold Langevin dynamics starting from $z = z_{\text{source}}$, with the drift term being the force term that drives the embedding toward z_{target} :

$$f_{\text{interp}}(z, z_{\text{target}}) = -\frac{z - z_{\text{target}}}{\|z - z_{\text{target}}\|_2} \quad (6)$$

In this case, we slightly modify the update rule of the Langevin dynamics (equation 3) as follows:

$$dz_t = \eta(\nabla_z f(z_t) + \lambda f_{\text{interp}}) + \sqrt{2\eta} \cdot \epsilon_t. \quad (7)$$

By setting the interpolation weight $\lambda > 0$ in equation 7, we add a directional bias that drives the latent trajectory toward the target point, while following the property gradients.

Results on interpolation Guided by a directional force toward a specified target, RNAGenScape generates smooth and coherent trajectories on the learned manifold while preserving biological plausibility and continuity (Figure S2). These trajectories connect arbitrary input-target sequence pairs in a structured manner, reflecting semantically meaningful transitions. The distances from each intermediate point to the source and target quantitatively demonstrate the monotonicity and smoothness of the interpolation (Figure S3).

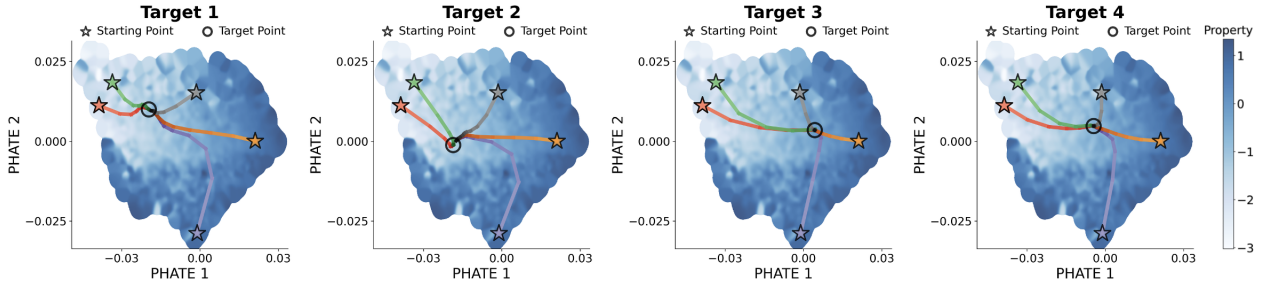


Figure S2. Latent space interpolation trajectories from 5 sources to 4 targets. Each trajectory is shown as a line fading from bright to dark in a consistent color. RNAGenScape produces smooth and coherent paths on the manifold between arbitrary input-target mRNA pairs.

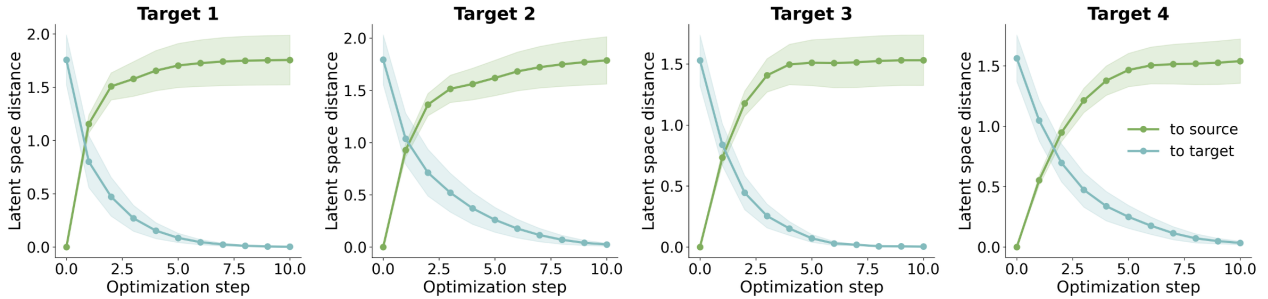


Figure S3. Latent space ℓ_2 distances during interpolation show smooth and monotonic transition from the source to the target. Results are averaged over all data samples.

E. Additional optimization trajectories

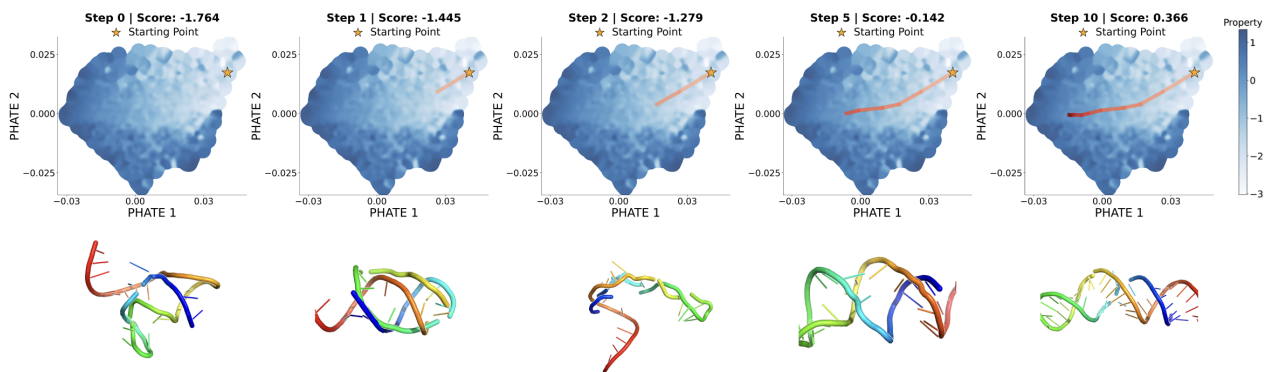


Figure S4. More examples of latent manifold trajectories. Trajectories in PHATE space and corresponding 3D structures are shown.

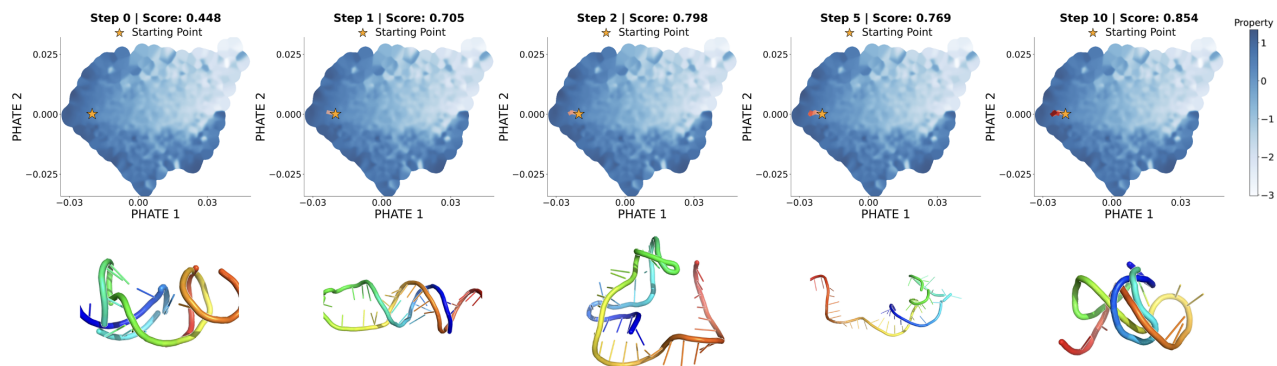


Figure S5. More examples of latent manifold trajectories. Trajectories in PHATE space and corresponding 3D structures are shown.

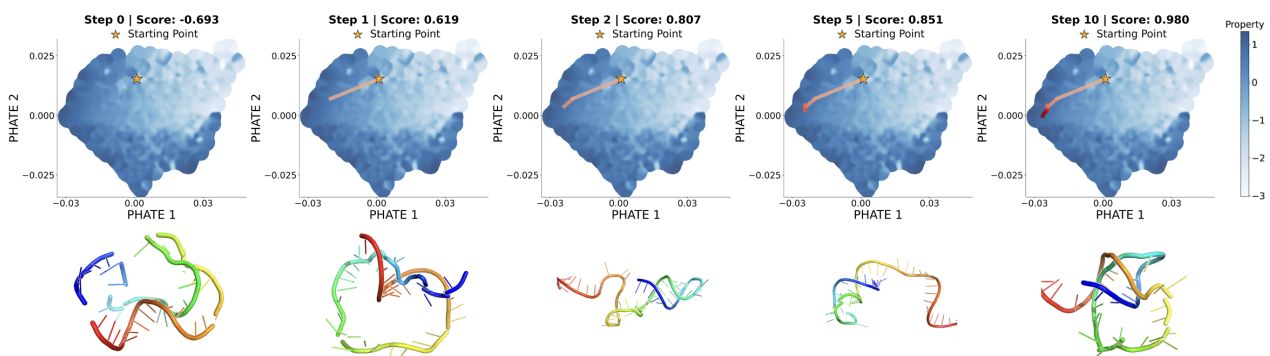


Figure S6. More examples of latent manifold trajectories. Trajectories in PHATE space and corresponding 3D structures are shown.

F. Extended Related Works

Sequence-to-function modeling A central goal in biological sequence modeling is predicting quantitative properties (e.g., expression level, stability) directly from the sequence (Oliver, 1996). Recent deep learning models trained on high-throughput experimental data have demonstrated strong performance in this setting, particularly for regulatory regions such as 5' UTRs and promoters (Sample et al., 2019; Vaishnav et al., 2022). Models such as ConvNets (Chen et al., 2024) and Transformers (He et al., 2023a) have been used to capture complex dependencies in mRNA space, and form the basis for downstream prediction of properties.

Generative models for design Generative models enable sampling of novel sequences enriched for desired traits. Variational autoencoders (VAEs) (Kingma et al., 2013) have been applied to proteins to learn smooth latent manifolds that are amenable to gradient-based optimization (Sinai et al., 2017; Castillo-Hair et al., 2024). ProteinMPNN (Dauparas et al., 2022), although described as a message-passing neural network by the authors, shares core design principles with autoencoders. Generative adversarial networks (Goodfellow et al., 2020) such as Méndez-Lucio et al. (Méndez-Lucio et al., 2020) or ProteinGAN (Wu et al., 2021) and autoregressive language models such as ProGen (Madani et al., 2023) have also been used to generate diverse protein sequences. More recently, diffusion models (Ho et al., 2020) have shown promise in discrete domains. For example, RFDiffusion (Watson et al., 2023) generates proteins unconditionally or conditioned on structural constraints. These methods can be readily adapted to mRNA design.

Optimization of biological sequences Sequence optimization can be framed as a black-box search or a differentiable surrogate-guided process. Several approaches relax discrete inputs for gradient-based updates, such as using straight-through estimators (Linder et al., 2019). ReLSO learns a continuous latent manifold and performs gradient ascent (Castro et al., 2022). Others apply reinforcement learning (Eastman et al., 2018) or Monte Carlo algorithm (Wirecki et al., 2023) for sequence optimization. Methods such as Fast SeqProp (Linder & Seelig, 2021) and LaMBO (Stanton et al., 2022) have demonstrated success in optimizing sequences under multi-objective constraints.

Integration of structural context While the present work strictly focuses on the mRNA sequence, many successful models incorporate inductive biases from the structures. ProteinMPNN (Dauparas et al., 2022) and diffusion-based inverse folding (Yi et al., 2023) condition sequence generation on 3D structures. ImmunoStruct (Givechian et al., 2025) jointly models protein sequence, structure, and biochemical properties to predict immunogenicity. CellSpliceNet (Afrasiyabi et al., 2025) integrates long-range sequence, local regions of interest, secondary structure, and gene expression to predict alternative splicing. EternaFold (Wayment-Steele et al., 2022) incorporate predicted secondary structures to improve fitness prediction. Although in our work we did not incorporate mRNA structures, extending RNAGenScape to sequence-structure joint modeling and optimization could be a promising direction.